








Long-duration Gamma-ray Burst and Associated Kilonova Emission from Fast-spinning Black Hole–Neutron Star Mergers

JIN-PING ZHU ¹, XIANGYU IVY WANG ^{2,3}, HUI SUN ⁴, YUAN-PEI YANG ⁵, ZHUO LI,^{1,6} RUI-CHONG HU ⁷,
YING QIN ⁸, AND SHICHAO WU ^{9,10}

¹*Department of Astronomy, School of Physics, Peking University, Beijing 100871, China; zhujp@pku.edu.cn*

²*School of Astronomy and Space Science, Nanjing University, Nanjing 210093, China*

³*Key Laboratory of Modern Astronomy and Astrophysics (Nanjing University), Ministry of Education, China*

⁴*Key Laboratory of Space Astronomy and Technology, National Astronomical Observatories, Chinese Academy of Sciences, Beijing 100012, People's Republic of China*

⁵*South-Western Institute for Astronomy Research, Yunnan University, Kunming, Yunnan 650500, People's Republic of China; ypyang@ynu.edu.cn*

⁶*Kavli Institute for Astronomy and Astrophysics, Peking University, Beijing 100871, China; zhuo.li@pku.edu.cn*

⁷*Guangxi Key Laboratory for Relativistic Astrophysics, School of Physical Science and Technology, Guangxi University, Nanning 530004, China*

⁸*Department of Physics, Anhui Normal University, Wuhu, Anhui, 241000, China*

⁹*Max-Planck-Institut für Gravitationsphysik (Albert-Einstein-Institut), D-30167 Hannover, Germany*

¹⁰*Leibniz Universität Hannover, D-30167 Hannover, Germany*

ABSTRACT

Gamma-ray bursts (GRBs) have been phenomenologically divided into long- and short-duration populations, generally corresponding to the collapsar and compact merger origin, respectively. Here we collect three unique bursts, GRBs 060614, 211211A and 211227A, all characterized by a long-duration main emission (ME) phase and a rebrightening extended emission (EE) phase, to study their observed properties and the potential origin as neutron star–black hole (NSBH) mergers. NS-first-born (BH-first-born) NSBH mergers tend to contain fast-spinning (non-spinning) BHs that more easily (hardly) allow tidal disruption to happen with (without) forming electromagnetic signals. We find that NS-first-born NSBH mergers can well interpret the origins of these three GRBs, supported by that: (1) Their X-ray MEs and EEs show unambiguous fall-back accretion signatures, decreasing as $\propto t^{-5/3}$, which might account for their long duration. The EEs can result from the fall-back accretion of r -process heating materials, predicted to occur after NSBH mergers. (2) The beaming-corrected local event rate density for this type of merger-origin long-duration GRBs is $\mathcal{R}_0 \sim 2.4^{+2.3}_{-1.3} \text{ Gpc}^{-3} \text{ yr}^{-1}$, consistent with that of NS-first-born NSBH mergers. (3) Our detailed analysis on the EE, afterglow and kilonova of the recently high-impact event GRB 211211A reveals it could be a merger between a $\sim 1.23^{+0.06}_{-0.07} M_{\odot}$ NS and a $\sim 8.21^{+0.77}_{-0.75} M_{\odot}$ BH with an aligned-spin of $\chi_{\text{BH}} \sim 0.62^{+0.06}_{-0.07}$, supporting an NS-first-born NSBH formation channel. Long-duration burst with rebrightening fall-back accretion signature after ME, and bright kilonova might be commonly observed features for on-axis NSBH mergers. We estimate the multimessenger detection rate between gravitational waves, GRB and kilonova emissions from NSBH mergers in O4 (O5) is $\sim 0.1 \text{ yr}^{-1}$ ($\sim 1 \text{ yr}^{-1}$).

Keywords: Gamma-ray bursts (629), Neutron stars (1108), Black holes (162), Gravitational waves (678)

1. INTRODUCTION

In observations, it is usually adopted that a critical duration of $T_{90} \sim 2 \text{ s}$ separates gamma-ray bursts (GRBs) into long- and short-duration populations (Norris et al. 1984; Kouveliotou et al. 1993). Long-duration GRBs (IGRBs) have been identified to be originated from massive collapsar by their association with broad-line Type

Ic supernovae (e.g., Galama et al. 1998; Woosley & Bloom 2006) and their exclusive hosts in star-forming galaxies (e.g., Bloom et al. 1998; Christensen et al. 2004). It has long been suspected that neutron star mergers, including binary neutron star (BNS) and neutron star–black hole (NSBH) mergers, are potential origins of short-duration GRBs (sGRBs; Paczynski 1986,

1991; Eichler et al. 1989; Narayan et al. 1992). Due to natal kicks imparted to the binaries at birth and long inspiral delays before mergers, NS mergers are believed to occur in low-density environments with significant offsets away from the centers of their host galaxies (e.g., Narayan et al. 1992; Bloom et al. 1999) supported by observations (e.g., Fong et al. 2010, 2015; Li et al. 2016). NS mergers can release an amount of neutron-rich matter (Lattimer & Schramm 1974, 1976; Symbalisty & Schramm 1982) that allows elements heavier than iron to be synthesized via the rapid neutron-capture process (r -process). It was predicted that the radioactive decay of these r -process nuclei would power an ultraviolet-optical-infrared thermal transient named “kilonova” (Li & Paczyński 1998; Metzger et al. 2010b).

The smoking-gun evidence for the BNS merger origin of sGRB and kilonova was the multimessenger observations of the first BNS merger gravitational-wave (GW) source GW170817 detected by the LIGO/Virgo Collaboration (LVC; Abbott et al. 2017a) and subsequent associated electromagnetic (EM) signals, including an sGRB GRB 170817A triggered by the Fermi Gamma-ray Burst Monitor (Abbott et al. 2017b; Goldstein et al. 2017; Savchenko et al. 2017; Zhang et al. 2018), a broadband jet afterglow from radio to X-ray with an off-axis viewing angle (e.g., Margutti et al. 2017; Troja et al. 2017; Lazzati et al. 2018; Lyman et al. 2018; Lamb et al. 2019; Ghirlanda et al. 2019) and a fast-evolving kilonova transient (AT2017gfo; e.g., Abbott et al. 2017c; Arcavi et al. 2017; Coulter et al. 2017; Drout et al. 2017; Evans et al. 2017; Kasliwal et al. 2017; Kilpatrick et al. 2017; Pian et al. 2017; Smartt et al. 2017). With the confirmation of the origin of sGRB and kilonova from the BNS merger population, one may especially expect to further establish the connection between NSBH mergers and their associated EM counterparts. However, although two high-confidence NSBHs (i.e., GW200105 and GW200115) and a few marginal NSBH GW candidates were detected during the third observing run of LVC (Abbott et al. 2021a; Nitz et al. 2021; The LIGO Scientific Collaboration et al. 2021), EM counterparts by the follow-up observations of these GWs were missing (e.g., Anand et al. 2021; Andreoni et al. 2020; Coughlin et al. 2020; Gompertz et al. 2020a; Kasliwal et al. 2020; Page et al. 2020), except an amphibious association between a subthreshold GRB GBM-190816 and a subthreshold NSBH event (Goldstein et al. 2019; Yang et al. 2020). One plausible explanation for the lack of detection of an EM counterpart is that present EM searches were too shallow to achieve distance and volumetric coverage for the probability maps of LVC events (Sagués Carracedo et al. 2021; Coughlin et al. 2020; Zhu et al. 2021b). Fur-

thermore, detailed studies on these NSBH candidates (Zhu et al. 2021a, 2022; Fragione 2021; Mandel & Smith 2021; Gompertz et al. 2022a; D’Orazio et al. 2022) revealed that they were more likely to be plunging events and could hardly produce any bright EM signals owing to near-zero spins of the primary BHs, since NSBH mergers tend to make tidal disruptions and drive bright EM counterparts if the primary BHs have high aligned-spins (e.g., Kyutoku et al. 2015; Foucart et al. 2018; Zhu et al. 2021a, 2022; Di Clemente et al. 2022).

Due to the lack of smoking-gun evidence, it is unclear whether NSBH mergers can contribute to the sGRB population (e.g., Gompertz et al. 2020b). On the one hand, the majority of NSBH binaries are believed to originate from the classic isolated binary evolution scenario (involving a common-envelope) (e.g., Giacobbo & Mapelli 2018; Belczynski et al. 2020; Drozda et al. 2020; Shao & Li 2021). In this scenario, the primary BHs are usually born first and have negligible spins consistent with the properties of LVC NSBH candidates (Broekgaarden & Berger 2021; Zhu et al. 2021a). Conversely, if the NSs are born first, the progenitors of the BHs would be tidally spun up efficiently by the NSs in close binaries (orbital periods $\lesssim 2$ d) and finally form fast-spinning BHs (Hu et al. 2022). A fraction of these NS-first-born NSBH systems formed in close binaries can merge within Hubble time. Therefore, compared with BH-first-born NSBH mergers, NS-first-born NSBH mergers are easier to allow tidal disruption to happen and drive bright GRB emissions. Because NS-first-born NSBH mergers may only account for $\lesssim 20\%$ NSBH populations (Román-Garza et al. 2021; Chattopadhyay et al. 2021, 2022), GRB populations contributed from NSBH mergers should be limited. On the other hand, most disrupted NSBH mergers can eject much more materials and lead to more powerful fall-back accretions than BNS mergers (Rosswog 2007; Fernández et al. 2017). Furthermore, r -process heating might affect the fall-back accretion of marginally bound matter (Metzger et al. 2010a). A late-time fall-back accretion of these materials may happen after tens of seconds of the merger if the remnant BH has a mass of $\gtrsim 6 - 8 M_{\odot}$. Because most NSBH mergers can remain BHs with masses in this range, Desai et al. (2019) suggested that an extended emission (EE) caused by the fall-back accretion of r -process heating materials can be an important signal to distinguish NSBH GRBs from BNS GRBs. Thus, it is plausible that the energy budgets, durations, and other observed properties of NSBH GRBs could differ from those of BNS mergers.

Very recently, the observations of an IGRB (i.e., GRB 211211A) associated with a kilonova emission at a

redshift $z = 0.0763$ (luminosity distance $D_L \approx 350$ Mpc) was reported by a few groups (Rastinejad et al. 2022; Yang et al. 2022; Xiao et al. 2022; Gompertz et al. 2022b; Mei et al. 2022; Zhang et al. 2022; Chang et al. 2022). The burst was characterized by a spiky main emission (ME) phase with a duration of ~ 13 s, an EE phase lasting ~ 55 s, and a temporal lull between these two phases. Since the observation property of its associated kilonova emission was similar to that of AT2017gfo¹ (Rastinejad et al. 2022; Xiao et al. 2022), indicating an origin of a compact binary coalescence, it was a challenge to interpret the intrinsically long duration of the burst. Yang et al. (2022) proposed that a merger of a near-equal-mass NS–white dwarf binary can well explain the ME of GRB 211211A, since the accretion of some high-angular-momentum white dwarf debris onto the remnant NS can prolong the burst duration. Gao et al. (2022) suggested a strong magnetic flux may surround the central engine of GRB 211211A, which results in the long-time accretion process due to the magnetic barrier effect (Proga & Zhang 2006; Liu et al. 2012).

Besides GRB 211211A, two other redshift-known (z -known) IGRBs, i.e., GRB 060614 and GRB 211227A, were proposed to derive from compact binary coalescences. GRB 060614 (Gal-Yam et al. 2006; Della Valle et al. 2006; Zhang et al. 2007) were found to be associated with a kilonova candidate (Yang et al. 2015), while GRB 211227A showed a large physical offset from the host center and lacked a supernova signature that should have been observed at the location of the burst (Lü et al. 2022). In this *Letter*, we study the properties of these three merger-origin IGRBs, especially for GRB 211211A, and show that a single explosive population via the NS-first-born NSBH merger can account for their origin. Here, the cosmological parameters are taken as $H_0 = 67.4 \text{ km s}^{-1} \text{ Mpc}^{-1}$, $\Omega_m = 0.315$, $\Omega_\Lambda = 0.685$ (Planck Collaboration et al. 2020).

2. PROPERTIES OF MERGER-ORIGIN IGRBS

2.1. Observed Properties and X-ray Fall-back Accretion Signals

We collect the observed data of three present z -known merger-origin IGRBs, including GRB 211221A (e.g., Rastinejad et al. 2022; Yang et al. 2022; Xiao et al. 2022), GRB 060614 (Gal-Yam et al. 2006; Della Valle et al. 2006; Zhang et al. 2007), and GRB 211227A (Lü

et al. 2022), all characterized by a spiky long-duration ME phase, a rebrightening EE phase, and a temporal lull between these two phases, to study their similarities. Here, the EE phase is defined as the long-lasting lower level emission phase after the initial intense ME phase (Norris & Bonnell 2006; Lan et al. 2020). The whole emission (WE) phase includes the ME phase and the EE phase. Table 1 lists the observed properties of the MEs and the WEs.

In the left panel of Figure 1, we divide detected GRBs into two populations, i.e., IGRB and sGRB populations, in the duration T_{90} vs. Earth-frame peak energy E_p diagram through the Gaussian mixture model. The intermediate population at the boundary region between IGRB and sGRB populations could be originated from collaspar or compact object coalescence (e.g., Tunnicliffe & Levan 2012; Zaninoni et al. 2016). Both MEs and WEs of these three merger-origin GRBs fall into the distribution of IGRBs. Therefore, without the redshift, host galaxy information, and associated kilonova detection, these three bursts would be classified as members of the IGRB population due to their long durations.

The correlations between the total isotropic equivalent energy $E_{\gamma, \text{iso}}$ of the prompt emission and the rest-frame peak energy $E_p(1+z)$ (Amati relation; Amati et al. 2002) for both IGRB and sGRB populations are shown in the right panel of Figure 1. We find that the WEs of these three bursts still behave as normal IGRBs, although their $E_{\gamma, \text{iso}}$ are lower than most observed IGRBs. Conversely, their MEs lie on the middle location of the sGRB track rather than on the IGRB track. The difference of $E_{\gamma, \text{iso}}$ between WEs and MEs, corresponding to the $E_{\gamma, \text{iso}}$ of the EEs, for these bursts are similar, which are $\sim 1 - 2 \times 10^{51}$ erg.

After a BNS/disrupted NSBH merger, a compact remnant accretion disk would be formed around the NS or BH. The lifetime of this disk is typically $\lesssim 1$ s, which is thought to determine the burst duration of an sGRB (e.g., Shapiro 2017; Zhang 2019; Ruiz et al. 2020). In order to explain the long durations of these three merger-origin GRBs, an additional energy/matter injection is needed. When a group of bound ejecta with an energy distribution of $dM/dE \propto E^\alpha$ where $\alpha \approx 0$ around $E = 0$ fall back onto the central NS or BH, the fall-back rate would track as $\propto t^{-5/3}$ (Rees 1988). As shown in Figure 2, we find that there are long-duration fall-back accretion signals appearing in the X-ray light curves of both MEs and EEs for these three bursts. The fall-back rates in their EEs peak at $\sim 20 - 40$ s and follow $\propto t^{-5/3}$ with a duration of $\sim 100 - 200$ s. Thus, the fall-back accretion might result in their long duration.

¹ Waxman et al. (2022) suggested that the burst could happen in another spatially nearby galaxy at a higher redshift. The near infrared emission following GRB 211211A could be thermal emission from dust, heated by UV radiation produced by the interaction between the jet plasma and the circumstellar medium, rather than a kilonova emission.

Table 1. The observed properties of GRB 211211A, GRB 060614¹, and GRB 211227A²

	GRB 211211A	GRB 060614	GRB 211227A
Main Emission			
Duration (s)	13	6	4
Peak energy (keV)	687^{+13}_{-11}	300^{+210}_{-90}	400^{+1200}_{-200}
Energy fluence (erg cm ⁻²)	$3.77^{+0.01}_{-0.01} \times 10^{-4}$	$8.2^{+0.6}_{-2.5} \times 10^{-6}$	$2.01^{+0.19}_{-0.42} \times 10^{-6}$
Isotropic equivalent energy (erg)	$5.30^{+0.01}_{-0.01} \times 10^{51}$	$3.18^{+0.22}_{-0.98} \times 10^{50}$	$2.69^{+0.25}_{-0.56} \times 10^{50}$
Spectral index α	$-0.996^{+0.005}_{-0.005}$	$-1.57^{+0.12}_{-0.14}$	$-1.56^{+0.15}_{-0.06}$
Spectral index β	$-2.36^{+0.02}_{-0.02}$
Whole Emission			
Duration (s)	$43.18^{+0.06}_{-0.06}$	102 ± 5	84
Peak energy (keV)	399^{+14}_{-16}	10 – 100	192^{+45}_{-42}
Energy fluence ³ (erg cm ⁻²)	$5.42^{+0.08}_{-0.08} \times 10^{-4}$	$4.09^{+0.18}_{-0.34} \times 10^{-5}$	$2.60^{+0.21}_{-0.21} \times 10^{-5}$
Isotropic equivalent energy (erg)	$7.61^{+0.11}_{-0.11} \times 10^{51}$	$1.59^{+0.07}_{-0.13} \times 10^{51}$	$3.48^{+0.16}_{-0.16} \times 10^{51}$
Spectral index α	$-1.20^{+0.01}_{-0.01}$...	$-1.34^{+0.10}_{-0.08}$
Spectral index β	$-2.05^{+0.02}_{-0.02}$...	$-2.26^{+0.24}_{-1.11}$
Redshift	0.076	0.125	0.228

¹ The data of GRB 211221A and GRB 060614 are collected from Table 1 of [Yang et al. \(2022\)](#).

² The data of GRB 211227A are collected from [Lü et al. \(2022\)](#) and [Tsvetkova et al. \(2022\)](#).

³ The energy fluence of the ME for GRB 211227A is calculated by the `HEASoft` tool ([Nasa High Energy Astrophysics Science Archive Research Center \(Heasarc\) 2014](#)) in the 15 – 1500 keV energy band.

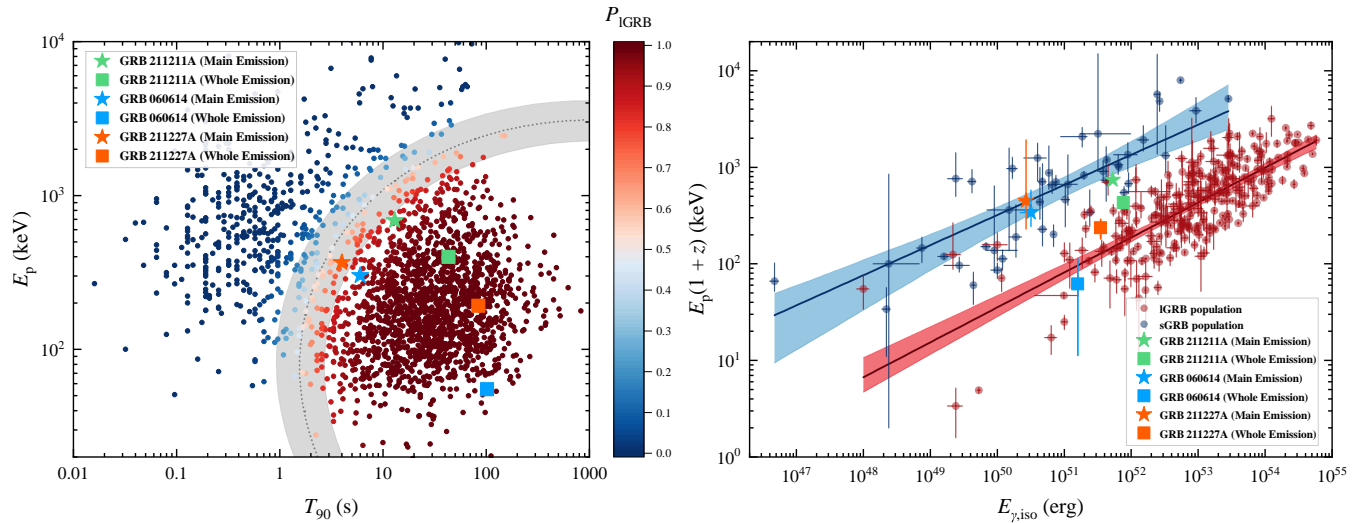


Figure 1. Left Panel: Long/short classification diagram in the $T_{90} - E_p$ domain ([von Kienlin et al. 2014](#); [Gruber et al. 2014](#); [Narayana Bhat et al. 2016](#); [von Kienlin et al. 2020](#)). The dashed line and gray shaded region are the best-fit and 1σ credible boundaries to distinguish IGRBs from sGRBs, respectively. The redder (bluer) the color of the point, the higher the possibility of the IGRB (sGRB) origin. Right Panel: $E_p(1+z)$ and $E_{\gamma,\text{iso}}$ correlation diagram with known redshift data ([Amati et al. 2002](#); [Zhang et al. 2009](#); [Minaev & Pozanenko 2020](#)). The red and blue solid lines represent the best-fit correlations for IGRB and sGRBs, respectively. The green, blue, and orange stars (squares) in both panels represent the placement of ME (WE) for GRB 211211A, GRB 060614, and GRB 211227A, respectively.

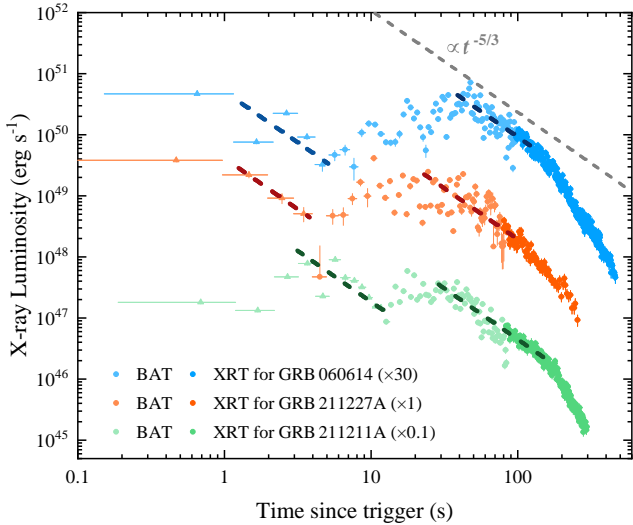


Figure 2. BAT and XRT light curves of GRB 211211A (green), GRB 060614 (blue) and GRB 211227A (orange). BAT luminosity is calculated at 10 keV. Their MEs and EEs are marked as triangle and circle points, respectively. The dashed lines represent the X-ray light curves track the $\propto t^{-5/3}$ mass fall-back accretion.

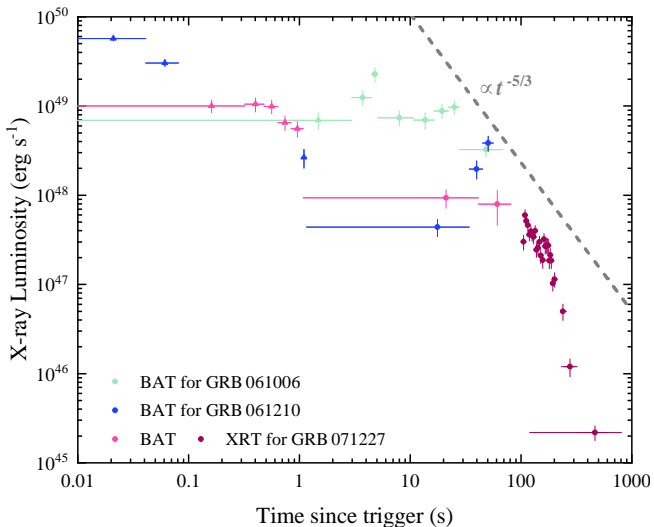


Figure 3. Similar to Figure 2, but for GRB 061006 (green), GRB 061210 (dark blue) and GRB 071227 (purple).

Gompertz et al. (2020a) collected 39 z -known sGRBs (7 events had an EE) and searched for possible NSBH candidates among these sGRBs. However, they didn’t find any clear evidences for the existence of NSBH GRBs in this complete sGRB sample. If a millisecond magnetar can survive after a BNS merger, the magnetar can lose its rotational energy via the spin-down process and result in a long-duration X-ray plateau in the X-ray lightcurve (Zhang & Mészáros 2001). Gompertz

et al. (2020a) presented that 4 of these sGRBs with EEs in their samples could be magnetar-like, so they cannot be originated from NSBH mergers. In Figure 3, we collect the X-ray light curve of other 3 sGRBs with EEs, including GRB 061006 (Berger 2007), GRB 061210 (Berger 2007) and GRB 071227 (D’Avanzo et al. 2009), whose X-ray emissions could not be well interpreted via the magnetar model by Gompertz et al. (2020a). We find that GRB 071227 could still be magnetar-like, characterized by a long-duration X-ray plateau. The X-ray lightcurves of GRB 061006 and GRB 061210 do not show any signatures of $\propto t^{-5/3}$ decay and hence may provide no evidence of unambiguous fall-back accretion signal, though that could be partly because of their limited data points. Thus, the EEs in present z -known sGRBs may not be caused by the fall-back accretions. The similar observed properties of merger-origin lGRBs, i.e., long durations and unambiguous rebrightening fall-back accretion signals, do not present in the existent observations of those of merger-origin sGRBs with/without EEs, indicating an unique origin for them.

In principle, both BNS and NSBH mergers can generate the early-time fall-back accretions (Rosswog 2007; Metzger et al. 2010a; Fernández et al. 2017). However, most of disrupted NSBH mergers would eject much more materials and lead to more powerful fall-back accretions than BNS mergers (Rosswog 2007). Furthermore, the simulations by Metzger et al. (2010a) and Desai et al. (2019) showed that r -process heating might affect on the materials that is marginally gravitationally bound. The gravity of the remnants formed after BNS mergers might be too low to drag these r -process heating materials back and result in fall-back accretions. However, as predicted by Desai et al. (2019), a late-time fall-back accretion of these materials may happen after tens of seconds of the merger if the remnant BH has a mass of $\gtrsim 6 - 8 M_{\odot}$, leading to a rebrightening emission with $t^{-5/3}$ power-law decay appeared in the X-ray lightcurve. The EEs of these three bursts, whose starting times and observational features are consistent with the predictions of Desai et al. (2019), may be originated from the fall-back accretion of r -process heating materials. We thus suspect that these three bursts are derived from NSBH mergers.

2.2. Event Rate Density

Assuming the unique merger origin of the three lGRBs, we investigate their local event rate density by tentatively constructing the luminosity function (LF) following Sun et al. (2015, 2022). The limited number of events can lead to large uncertainty of the LF. However, it can be plausible to make a fine evaluation by

adding up the contribution of all three events. Following the Equation (12) in Sun et al. (2022), the LF $\Phi(L)$ is the sum of each event j in the range from $\log_{10} L$ to $\log_{10} L + d \log_{10} L$ (with total ΔN_L events).

$$\begin{aligned} \Phi(L)d \log_{10} L &= \sum_{j=1}^{\Delta N_L} [\Phi(L)d \log_{10} L]_j \\ &= \sum_{j=1}^{\Delta N_L} \frac{1}{[T_{\text{BAT}} \times V'_{\text{max}}]_j}, \end{aligned} \quad (1)$$

where T_{BAT} is the total monitoring time by Swift/BAT and V'_{max} is the effective maximum volume that is monitored (with field of view Ω_{BAT}) weighted by the density evolution $f(z)$ and time dilation, i.e.,

$$V'_{\text{max}} = \int_0^{z_{\text{max}}} \frac{\Omega_{\text{BAT}}}{4\pi} \cdot \frac{f(z)}{1+z} \frac{dV(z)}{dz} dz. \quad (2)$$

The z_{max} is the maximum redshift that an event can be detected with bolometric peak luminosity L_{bol} . The bolometric peak luminosity of these three events, defined in the energy range of $1 - 10^4$ keV, are derived from k -correction based on the spectrum listed in Table 1 following Equation (29) in Sun et al. (2015).

We take the instrument parameters of Swift/BAT with $\Omega_{\text{BAT}} = 1.3$, $T_{\text{BAT}} = 17$ yr and the flux sensitivity $f_{\text{th,BAT}} = 3 \times 10^{-8}$ erg cm $^{-2}$ s $^{-1}$. The $f(z)$ for GRBs with merger-origin is adopted from Zhu et al. (2021b). We take the correction of the redshift measurement into account. For both the IGRBs and sGRBs sample, the ratio between the total number and the number of z -known events from the Swift observations is approximately 4 : 1. In addition, since Swift has relatively softer energy band than BATSE, it tends to detect more IGRBs than sGRBs. One needs to adopt another correction by a factor of 3 to compensate the short (hard)-to-long (soft) ratio of Swift-detected GRBs in comparison to those by BATSE observations (Sun et al. 2015).

We divided the events into two bins with $\Delta \log_{10} L = 1$ and fitted the LF with a single power law of the slope 0.6 ± 0.8 . The local event rate density, which is derived by integrating the LF above the luminosity threshold 3×10^{50} erg s $^{-1}$, is given as

$$\mathcal{R}_0(> 3 \times 10^{50} \text{ erg s}^{-1}) = 2.4_{-1.3}^{+2.3} \times 10^{-2} \text{ Gpc}^{-3} \text{ yr}^{-1}. \quad (3)$$

The errors are given at the 1σ confidence level (Gehrels 1986).

The intrinsic local event rate densities of both IGRBs and sGRBs are of the order of unity in unit of $\text{Gpc}^{-3} \text{ yr}^{-1}$ above the isotropically bolometric luminosity of $\sim 10^{50}$ erg s $^{-1}$ (Sun et al. 2015). We find that the local event rate density for the IGRBs with

merger origin is much lower than that of both IGRBs or sGRBs. The rate density for BNS inferred using GWs through GWTC-2 (GWTC-3) is $320_{-240}^{+490} \text{ Gpc}^{-3} \text{ yr}^{-1}$ ($10 - 1700 \text{ Gpc}^{-3} \text{ yr}^{-1}$) (e.g., Abbott et al. 2021b; The LIGO Scientific Collaboration et al. 2021; Mandel & Broekgaarden 2022). Abbott et al. (2021a) inferred a NSBH rate density of $45_{-33}^{+75} \text{ Gpc}^{-3} \text{ yr}^{-1}$ by considering the observations of two NSBH mergers or $130_{-69}^{+112} \text{ Gpc}^{-3} \text{ yr}^{-1}$ assuming a broad NSBH population, while GWTC-3 (The LIGO Scientific Collaboration et al. 2021) reported the NSBH merger rate density to be between $7.8 - 140 \text{ Gpc}^{-3} \text{ yr}^{-1}$. By considering a jet beaming factor of $f_b = 0.01$, the beaming-corrected event rate density for merger-origin IGRBs is $\mathcal{R}_{0,b} = 2.4_{-1.3}^{+2.3} (f_b/0.01) \text{ Gpc}^{-3} \text{ yr}^{-1}$, which is much lower than those of BNS and NSBH mergers. However, the beaming-corrected rate density of merger-origin IGRBs is consistent with that of NS-first-born NSBH merger ($\lesssim 20\%$ of total NSBH populations; Román-Garza et al. 2021; Chattopadhyay et al. 2022). By investigating the parameter space of forming NS-first-born NSBH binaries, Hu et al. (2022) found that most of NSBH binaries that can merge within Hubble time would have BHs with projected aligned spins $\chi_{\text{BH}} \gtrsim 0.8$ and, hence, can certainly make tidal disruptions to produce electromagnetic counterparts. Only a small fractional low-mass BHs with $\chi_{\text{BH}} \sim 0.2 - 0.8$ can merge with an NS within Hubble time and can still allow tidal disruption to happen if NSs are not really massive (i.e., $M_{\text{NS}} \gtrsim 1.6 - 2.0 M_{\odot}$). Since the rest of BH-first-born NSBH mergers would mostly contribute to plunging events due to negligible projected aligned-spins of BH components (Zhu et al. 2022), a single explosive population via the NS-first-born NSBH merger can account for their origin.

3. MODELING AND ORIGIN OF GRB211211A

GRB211211A, as a recently high-impact event, had one of the most complete multi-band data records of afterglow and kilonova, which can give a strict constraint on our fitting parameters to explore its plausible origin. In this section, we will simultaneously interpret the emissions of γ -ray/X-ray EEs by the fall-back accretion of r -process heating materials, afterglow emissions, and kilonova emissions of GRB211211A, within the framework of NSBH mergers. Since the structures of the prompt emissions of GRBs are generally believed to originate from the internal shock processes, in the following discussion, we are only interested in the light curve outline that mainly depends on the engine power due to the fall-back accretion.

3.1. Modeling

3.1.1. Fall-back Accretion of r -process Heating Materials

For NSBH mergers with NS tidal disruption, a fractional of r -process heating materials would fall back onto the remnant BH tens of seconds after the merger, resulting in the EE (Metzger et al. 2010a; Desai et al. 2019) through the Blandford-Znajek (BZ) mechanism (Blandford & Znajek 1977). Following MacFadyen et al. (2001) and Dai & Liu (2012), the fall-back rate initially increases with time as $\dot{M} \propto t^{1/2}$ before the time of t_p corresponding to the peak fall-back rate \dot{M}_p . Then, the late-time fall-back accretion behavior would track as $\dot{M} \propto t^{-5/3}$ until the break time t_b (Chevalier 1998). While most of fall-back materials are accreted after t_b , we describe the fall-back rate as $\dot{M} \propto t^{-s}$. An empirical three-segment broken power-law function is adopted to model the fall-back accretion rate of r -process heating materials, i.e.,

$$\dot{M}(t) = \dot{M}_p \left[\frac{1}{2} \left(\frac{t-t_0}{t_p-t_0} \right)^{-1/2} + \frac{1}{2} \left(\frac{t-t_0}{t_p-t_0} \right)^{5/3} \right]^{-1} \times \left[1 + \frac{1}{2} \left(\frac{t-t_0}{t_b-t_0} \right)^{s-5/3} \right]^{-1}, \quad (4)$$

where t_0 is the starting time of the fall-back accretion.

The BZ power is related to the mass and spin of the central BH (e.g., Li & Paczyński 2000; Wu et al. 2013; Lei et al. 2013, 2017; Liu et al. 2017), i.e.,

$$L_{\text{BZ}} = 1.7 \times 10^{50} \text{ erg s}^{-1} \chi_{\text{BH}} \left(\frac{M_{\text{BH}}}{M_{\odot}} \right)^2 B_{\text{BH},15}^2 F(\chi_{\text{BH}}), \quad (5)$$

where M_{BH} is the central BH mass, χ_{BH} is the dimensionless aligned-spin of the BH, $B_{\text{BH},15} = B_{\text{BH}}/10^{15} \text{ G}$ is the magnetic field strength threading the BH horizon and $F(\chi_{\text{BH}}) = [(1+q^2)/q^2][(q+1/q)\arctan q - 1]$ with $q = \chi_{\text{BH}}/(1 + \sqrt{1 - \chi_{\text{BH}}^2})$. The magnetic field can be estimated through the balance between the magnetic pressure on the horizon and the ram pressure of the innermost part of the accretion flow:

$$\frac{B_{\text{BH}}^2}{8\pi} = P_{\text{ram}} \sim \rho c^2 \sim \frac{\dot{M}c}{4\pi r_{\text{H}}^2}, \quad (6)$$

where c is the speed of light and $r_{\text{H}} = (1 + \sqrt{1 - \chi_{\text{BH}}^2})r_{\text{g}}$ is the radius of the BH horizon with the Schwarzschild radius $r_{\text{g}} = GM_{\text{BH}}/c^2$ and the gravitational constant G . Thus, the BZ power can be also expressed as

$$L_{\text{BZ}} = 9.3 \times 10^{53} \text{ erg s}^{-1} \frac{\chi_{\text{BH}}^2 F(\chi_{\text{BH}})}{(1 + \sqrt{1 - \chi_{\text{BH}}^2})^2} \frac{\dot{M}}{M_{\odot} \text{ s}^{-1}}. \quad (7)$$

Because the central BH would be spun up by accretion and spun down by the BZ mechanism, the conservation of energy and angular momentum of a BH can be written as

$$\begin{aligned} \frac{dM_{\text{BH}}c^2}{dt} &= \dot{M}c^2 E_{\text{ISCO}} - L_{\text{BZ}}, \\ \frac{dJ_{\text{BH}}}{dt} &= \dot{M}J_{\text{ISCO}} - 2L_{\text{BZ}}/\Omega_{\text{H}}, \end{aligned} \quad (8)$$

where $\Omega_{\text{H}} = c\chi_{\text{BH}}/(2r_{\text{H}})$ is the angular velocity of the BH horizon, $E_{\text{ISCO}} = (4\sqrt{\tilde{R}_{\text{ISCO}}} - 3\chi_{\text{BH}})/\sqrt{3\tilde{R}_{\text{ISCO}}}$ and $J_{\text{ISCO}} = 2GM_{\text{BH}}(3\sqrt{\tilde{R}_{\text{ISCO}}} - 2\chi_{\text{BH}})/c\sqrt{3\tilde{R}_{\text{ISCO}}}$ are the specific energy and specific angular momentum of a particle at the innermost stable circular orbit (ISCO) radius (Novikov & Thorne 1973), respectively. $\tilde{R}_{\text{ISCO}} = 3 + Z_2 - \text{sign}(\chi_{\text{BH}})\sqrt{(3 - Z_1)(3 + Z_1 + 2Z_2)}$ represents the normalized radius of the BH ISCO with $Z_1 = 1 + (1 - \chi_{\text{BH}}^2)^{1/3}[(1 + \chi_{\text{BH}})^{1/3} + (1 - \chi_{\text{BH}})^{1/3}]$ and $Z_2 = \sqrt{3\chi_{\text{BH}}^2 + Z_1^2}$ (Bardeen et al. 1972). Since the angular momentum of BH is expressed as $J_{\text{BH}} = GM_{\text{BH}}^2\chi_{\text{BH}}/c$, one has

$$\begin{aligned} \frac{d\chi_{\text{BH}}}{dt} &= \frac{(\dot{M}J_{\text{ISCO}} - 2L_{\text{BZ}}/\Omega_{\text{H}})c}{GM_{\text{BH}}^2} \\ &\quad - \frac{2\chi_{\text{BH}}(\dot{M}c^2 E_{\text{ISCO}} - L_{\text{BZ}})}{M_{\text{BH}}c^2}. \end{aligned} \quad (9)$$

By combing Equations (7), (8) and (9), the time-evolving BZ power can thus be calculated. The observed γ -ray/X-ray light curve caused by the fall-back accretion is connected to the BZ power via the γ -ray/X-ray radiation efficiency $\eta_{(\gamma,\text{X})}$ and the jet beaming factor f_{b} , i.e.,

$$\eta_{(\gamma,\text{X})}L_{\text{BZ}} = f_{\text{b}}L_{(\gamma,\text{X})}. \quad (10)$$

3.1.2. Jet Afterglow Emissions

In order to calculate the afterglow light curves, we adopt the Gaussian structured jet model (e.g., Zhang & Mészáros 2002) which was favored by the observations of GRB 170817A afterglow (e.g., Lamb & Kobayashi 2018; Lazzati et al. 2018; Mooley et al. 2018; Troja et al. 2018; Xie et al. 2018), i.e.,

$$E(\theta) = E_0 \exp\left(-\frac{\theta^2}{2\theta_c^2}\right), \quad (11)$$

where E_0 is the on-axis equivalent isotropic energy and θ_c is the characteristic core angle. The spectra of the standard synchrotron emission from relativistic electrons are employed following Sari et al. (1998); Kumar & Zhang (2015) and Zhang (2018). For more details of the afterglow modeling we applied to calculate the sGRB

light curves along the line of sight, see Appendix C in [Zhu et al. \(2021b\)](#). We constrain the afterglow parameters, including E_0 , θ_c , viewing angle θ_v with respect to the moving direction of the jet, circumburst number density n , power-law index of the electron distribution p , $\bar{\alpha}$ and fraction of shock energy carried by magnetic fields ε_B , to fit the multi-band light curves of GRB 211211A. The fraction of shock energy carried by electrons is set to its typical value of $\varepsilon_e = 0.1$.

3.1.3. Ejecta Mass

After NSBH mergers, a fraction of neutron-rich matter (i.e., an unbound dynamical ejecta) is tidally ejected while an accretion disk is formed around the remnant BH. The total remnant mass outside the remnant and the dynamical ejecta mass are dependent on the NSBH system parameters, including the BH mass M_{BH} , the dimensionless spin parameter projected onto the orientation of orbital angular momentum χ_{BH} , the NS mass M_{NS} , and the NS equation of state (EoS), which can be calculated based on an empirical fitting formula, i.e.,

$$\frac{M_{\text{fit}}}{M_{\text{NS}}^{\text{b}}} = \left[\max \left(a_1 \frac{1 - 2C_{\text{NS}}}{\eta^{1/3}} - a_2 \tilde{R}_{\text{ISCO}} \frac{C_{\text{NS}}}{\eta} + a_3, 0 \right) \right]^{a_4}, \quad (12)$$

where M_{NS}^{b} is the baryonic mass of the NS, C_{NS} is the compactness of the NS determined by the NS EoS, $\eta = Q/(1 + Q)^2$, and $Q = M_{\text{BH}}/M_{\text{NS}}$ is the mass ratio between the primary BH mass and the secondary NS mass. For the fitting formula of the total remnant mass $M_{\text{tot,fit}}$ (the dynamical ejecta mass $M_{\text{d,fit}}$), the parameters in Equation (12) are $a_1 = 0.406$, $a_2 = 0.139$, $a_3 = 0.255$, and $a_4 = 1.761$ ($a_1 = 0.218$, $a_2 = 0.028$, $a_3 = -0.122$, and $a_4 = 1.358$) obtained from [Foucart et al. \(2018\)](#) ([Zhu et al. 2020](#)). Since the fitting formulas of the total remnant mass and the dynamical ejecta mass are obtained with independent simulation data, one needs to set an upper limit on the maximum fraction of dynamical ejecta mass to the total remnant mass, i.e., $M_{\text{d,max}} \approx f_{\text{max}} M_{\text{total,fit}}$. We set $f_{\text{max}} \approx 0.5$ based on simulation results from [Kyutoku et al. \(2015\)](#). Therefore, the final empirical mass of the dynamical ejecta is $M_{\text{d}} \approx \min(M_{\text{d,fit}}, f_{\text{max}} M_{\text{total,fit}})$.

We consider two ejecta components for NSBH kilonova model, i.e., the wind ejecta from the disk around the remnant BH and the dynamical ejecta caused by tidal forces. The wind ejecta mass can be estimated as a constant fraction of the disk mass, i.e., $M_{\text{w}} \approx \xi_{\text{w}} M_{\text{disk}}$, where $\xi_{\text{w}} \approx 0.2$ ([Fernández et al. 2015](#); [Just et al. 2015](#); [Siegel & Metzger 2017](#)).

Numerical simulations revealed that the dynamical ejecta from NSBH mergers are highly anisotropic and distributed in the equatorial plane ([Kyutoku et al. 2015](#);

[Kawaguchi et al. 2016](#); [Darbha et al. 2021](#)). [Zhu et al. \(2020\)](#) constructed a viewing-angle-dependent model for NSBH kilonovae and found that the wind ejecta can be covered by the dynamical ejecta for a large θ_v condition. However, for the case of GRB 211211A observed in the on-axis or near-on-axis view (i.e., $\theta_v \sim 0^\circ$), one can simultaneously see two components. Hereafter, in order to reduce computational complexity, we used a simplified model based on [Zhu et al. \(2020\)](#) to separately consider the emissions from the wind ejecta and the dynamical ejecta.

Assuming that the wind ejecta has an isotropic density profile and a homologous expansion, we adopt the common analytic solution derived by [Arnett \(1982\)](#) and [Chatzopoulos et al. \(2012\)](#) to calculate the bolometric luminosity of the wind ejecta:

$$L_{\text{w}}(t) = e^{-(t'/t_{\text{w,diff}})^2} \int_0^t 2L_{\text{w,in}}(t') \frac{t'}{t_{\text{w,diff}}} e^{(t'/t_{\text{w,diff}})^2} \frac{dt'}{t_{\text{w,diff}}}, \quad (13)$$

where $t_{\text{w,diff}} = (2\kappa_{\text{w}} M_{\text{w}} / \beta v_{\text{w}} c)^{1/2}$ is the photon diffusion timescale of the wind ejecta, κ_{w} is the grey opacity, and $\beta = 13.8$ is the dimensionless constant. $L_{\text{w,in}}(t) = \epsilon_{Y_e} \epsilon_{\text{th}} \dot{\epsilon}(t) M_{\text{w}}$ represents the injection heating rate from the radioactive decay of r -process nucleus, where $\epsilon_{Y_e} = 0.5 + 2.5[1 + e^{4(t/\text{day}-1)}]^{-1}$ if $Y_e \leq 0.25$ ($\epsilon_{Y_e} = 1$ otherwise) is an electron-fraction-dependent term which takes into account extremely neutron-rich ejecta with a decay half-life of a few hours ([Perego et al. 2017](#)), $\epsilon_{\text{th}} \approx 0.5$ is the efficiency of thermalization ([Metzger et al. 2010b](#)), and $\dot{\epsilon}(t) = \dot{\epsilon}_0(t/\text{day})^{-\alpha}$ is the specific energy injection rate due to radioactive decay with $\dot{\epsilon}_0 \approx 1.58 \times 10^{10} \text{ erg g}^{-1} \text{ s}^{-1}$ and $\alpha \approx 1.3$ ([Korobkin et al. 2012](#)).

In order to calculate the monochromatic light curves of the wind ejecta, we define an photosphere temperature as

$$T_{\text{w,phot}}(t) = \max \left[\left(\frac{L_{\text{w}}(t)}{4\pi\sigma_{\text{SB}}v_{\text{w}}^2 t^2} \right)^{1/4}, T_{\text{La}} \right]. \quad (14)$$

where σ_{SB} is the Stefan-Boltzmann constant, $v_{\text{w}} \approx 0.067c$ is assumed to be the wind ejecta velocity (e.g., [Just et al. 2015](#); [Siegel & Metzger 2017](#); [Perego et al. 2017](#)), and $T_{\text{La}} \approx 1000 \text{ K}$ is the first ionisation temperature of lanthanides ([Barnes & Kasen 2013](#)). The photosphere radius can be written as

$$R_{\text{w,phot}}(t) = \begin{cases} v_{\text{w}} t, & \text{for } T_{\text{w,phot}} > T_{\text{La}}, \\ \left(\frac{L_{\text{w}}(t)}{4\pi\sigma_{\text{SB}}T_{\text{La}}^4} \right)^{1/2}, & \text{for } T_{\text{w,phot}} = T_{\text{La}}, \end{cases} \quad (15)$$

Then, the flux density contributed from the emission of the wind ejecta is given by

$$F_{\nu,w} = \frac{8\pi^2 R_{w,\text{phot}}^2}{h^2 c^2} \frac{h^3 \nu^3}{\exp(h\nu/k_B T_{w,\text{phot}} - 1)} \frac{1}{4\pi D_L^2}, \quad (16)$$

where h , k_B and ν represent the Planck constant, the Boltzmann constant and frequency, respectively.

Based on the simulations of NSBH mergers (Kyutoku et al. 2015), the mass distribution of dynamical ejecta is highly anisotropic, with the mass mainly distributed around the equatorial plane and shaped like a crescent. The dynamical ejecta is typically concentrated around the orbital plane with a half opening angle in the latitudinal direction of $\theta_d \approx 15^\circ$ and often sweeps out only a half of the plane, i.e., an opening angle in the longitudinal direction of $\varphi_d \approx 180^\circ$. Since the dynamical ejecta is geometrically thin in the latitudinal direction, the photons would be always diffused from the latitudinal edge. Due to $dM_d/dv \approx \text{const}$ between the radial velocity range of $v_{d,\text{min}} < v < v_{d,\text{max}}$ based on the numerical relativity simulations (Kyutoku et al. 2015), the bolometric luminosity of the dynamical ejecta can be obtained from Kawaguchi et al. (2016), i.e.,

$$L_d(t) \approx (1 + \theta_d) \epsilon_{\text{th}} \epsilon_0 M_d \times \begin{cases} \left(\frac{t}{t_c} \left(\frac{t}{\text{day}}\right)\right)^{-\alpha}, & \text{for } t < t_c, \\ \left(\frac{t}{\text{day}}\right)^{-\alpha}, & \text{for } t > t_c, \end{cases} \quad (17)$$

where $t_c = [\kappa_d \theta_d M_d / 2c\varphi_d (v_{d,\text{max}} - v_{d,\text{min}})]^{1/2}$ is defined as the critical diffuse timescale that all ejecta can be seen. We set the minimum velocity $v_{d,\text{min}} \approx 0.1c$ following the simulations of Kyutoku et al. (2015) while the maximum velocity can be estimated as $v_{d,\text{max}} = \sqrt{3v_{d,\text{rms}}^2 - 3v_{d,\text{min}}^2/4} - v_{d,\text{min}}/2$ where $v_{d,\text{rms}} = (-0.441Q^{-0.224} + 0.539)c$ is the root-mean-square velocity of the dynamical ejecta obtained from Zhu et al. (2020).

Because $dL_d/2$ is released over an area of $\varphi_d v t^2 dv$, one can derive the photosphere temperature of each velocity at a given time:

$$T_{d,\text{phot}}(v, t) \approx \left[\frac{L_d(t)}{2\sigma_{\text{SB}} \varphi_d v (v_{d,\text{max}} - v_{d,\text{min}}) t^2} \right]^{1/4}. \quad (18)$$

The total flux density from the dynamical ejecta can be expressed as

$$F_{\nu,d} \approx \int_{v_{d,\text{min}}}^{v_{d,\text{max}}} \frac{4\pi \varphi_d v t^2}{h^2 c^2} \frac{h^3 \nu^3}{\exp(h\nu/k_B T_{d,\text{phot}} - 1)} \frac{1}{4\pi D_L^2} dv. \quad (19)$$

3.2. Origins of GRB 211211A and Associated Kilonova

Table 2. Priors and Results for Fitting Parameters

Parameter	Prior	Min	Max	Result
M_{BH}/M_\odot	Flat	2.22	15	$8.21_{-0.75}^{+0.77}$
χ_{BH}	Flat	0	0.997	$0.62_{-0.07}^{+0.06}$
M_{NS}/M_\odot	Gaussian	1.0	2.22	$1.23_{-0.07}^{+0.06}$
$\kappa_w/\text{cm}^2\text{g}^{-1}$	Flat	0.5	5	$0.56_{-0.05}^{+0.13}$
$\kappa_d/\text{cm}^2\text{g}^{-1}$	Flat	10	100	$11.0_{-0.8}^{+1.4}$
$\dot{M}_p/M_\odot\text{s}^{-1}$	Log-flat	10^{-10}	1	$2.19_{-0.37}^{+0.44} \times 10^{-5}$
t_0/s	Log-flat	10	12.7	$11.2_{-0.0}^{+0.0}$
t_p/s	Log-flat	12.7	40	$30.2_{-0.0}^{+0.0}$
t_b/s	Log-flat	100	1000	234_{-0}^{+0}
s	Flat	0	15	$7.33_{-0.19}^{+0.19}$
η_γ	Log-flat	10^{-2}	1	$0.29_{-0.00}^{+0.00}$
E_0/erg	Log-flat	10^{50}	10^{53}	$5.1_{-1.9}^{+2.6} \times 10^{52}$
θ_c/rad	Flat	0	0.2	$0.03_{-0.00}^{+0.00}$
θ_v/rad	Flat	0	0.5	$0.07_{-0.01}^{+0.01}$
p	Flat	2	3	$2.01_{-0.01}^{+0.01}$
$n/\text{g cm}^{-3}$	Log-flat	10^{-6}	2	$0.41_{-0.30}^{+0.77}$
ϵ_B	Log-flat	10^{-5}	1	$1.3_{-0.6}^{+1.8} \times 10^{-3}$

NOTE—The prior of M_{NS} is adopted as a Gaussian distribution, i.e., $\mathcal{N}(M_{\text{NS}}/M_\odot) \sim (\mu = 1.3, \sigma = 0.11)$, consistent with the observed mass distribution of NSs in Galactic BNS systems (Lattimer 2012).

For simplicity, we directly use the final BH mass $M_{\text{BH},f}$ and final dimensional aligned-spin $\chi_{\text{BH},f}$ after NSBH mergers based on Equation (3) and Equation (5) from Deng (2020) as functions of the initial NSBH system parameters, i.e., M_{BH} , M_{NS} , C_{NS} and χ_{BH} , to determine the BZ power. The observed mass distribution of Galactic BNS systems (Lattimer 2012) were inferred to be a Gaussian distribution, i.e., $\mathcal{N}(M_{\text{NS}}/M_\odot) \sim (\mu = 1.3, \sigma = 0.11)$. The observations of GW200105 and GW200115 showed that their NS masses are $\sim 1.9 M_\odot$ and $\sim 1.5 M_\odot$ (Abbott et al. 2021a), plausibly more massive than the mass distribution of Galactic BNS systems. Furthermore, some population synthesis simulations predicted that NSBH mergers might usually contain more massive NSs compared to those in BNS mergers (e.g., Giacobbo & Mapelli 2018; Broekgaarden et al. 2021). However, due to currently limited observations for NSBH GWs that could hardly represent a complete mass distribution of NSs in NSBH mergers, we use the observed mass distribution of NSs in Galactic BNS systems as the prior of NS mass. Here, an EoS of AP4 (Akmal & Pandharipande 1997) is adopted since it is one of the most likely EoSs constrained by GW170817 (Abbott

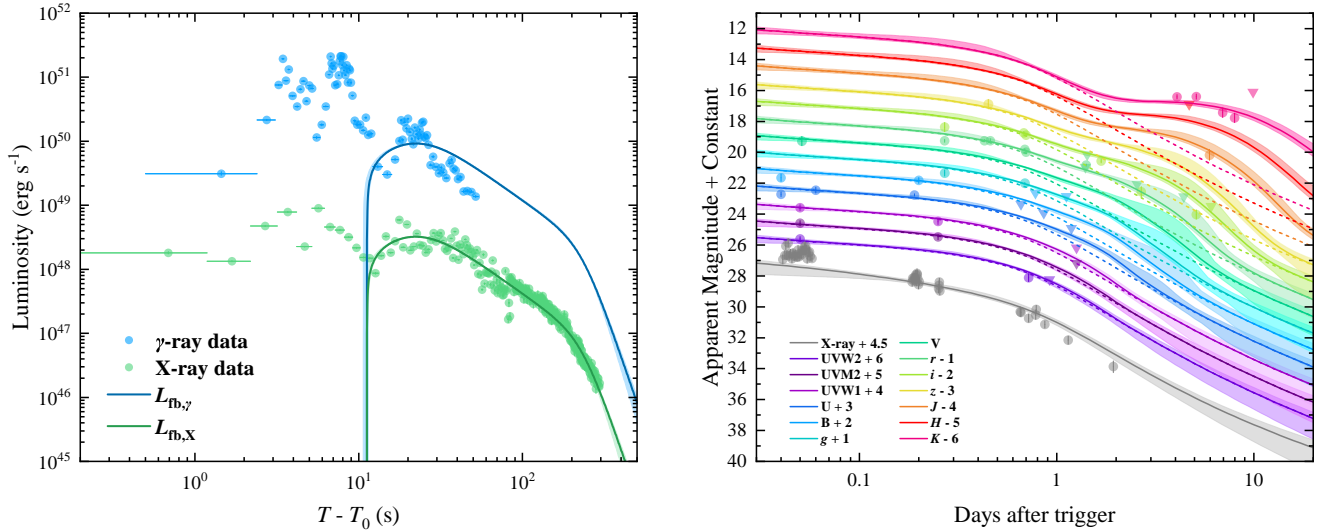


Figure 4. Left panel: γ -ray (blue points from Yang et al. 2022) and X-ray (green points from BAT and XRT) light curves of GRB 211211A. Blue and green lines are the fittings of the EEs using the fall-back accretion model. Right panel: the detections (circle points) and upper limits (inverted triangle points) of the multi-band data for GRB 211211A afterglow and associated kilonova emissions. The solid lines and shaded areas represent the best-fittings and 90% credible intervals for the multi-band data, while the contributions from the afterglow emissions are marked as the dashed lines.

et al. 2018). In our calculations, we set $\eta_\gamma = 0.01$ and $f_b = 0.01$ while η_γ is assumed to be a fitting parameter.

In theory, NSBH kilonovae were thought to be optically dim, but infrared bright compared with BNS kilonovae (e.g., Kasen et al. 2017; Kawaguchi et al. 2020; Zhu et al. 2020), because the NSBH merger probably produces a large number of lanthanide-rich dynamical ejecta with opacity $\kappa_d \sim 10 - 100 \text{ cm}^2 \text{ g}^{-1}$. The disk wind ejecta is hardly to be lanthanide-poor due to the lack of shock heating and neutrino irradiation during or shortly after the merger (e.g., Just et al. 2015; Fernández et al. 2015). However, Fujibayashi et al. (2020) and Kyutoku et al. (2020) recently found that the wind ejecta can still be lanthanide-poor if the viscous coefficient is not extremely high. Given the uncertainty of the wind ejecta, we adopt a wide prior distribution for the wind ejecta opacity, which is $\kappa_w \sim 0.5 - 5 \text{ cm}^2 \text{ g}^{-1}$.

There are 17 free parameters summarized in Table 2. The Markov Chain Monte Carlo method with the `emcee` package (Foreman-Mackey et al. 2013) is adopted to simultaneously fit the data of γ -ray/X-ray EE, afterglow, and kilonova emissions of GRB 211211A. We summarize the total 17 free parameters and their fitting results with 1σ credible intervals in Table 2, while the posteriors of these fitting parameters are shown in Figure 5. Except κ_w and κ_d , these fitting parameters are convergent. The lower value of κ_w indicates that the wind ejecta of NSBH mergers could be lanthanide-poor. The best-fit light curves of γ -ray/X-ray EE, afterglow, and kilonova emissions are shown in Figure 4.

Our fitting results reveal that GRB 211211A could be a merger between a $\sim 1.23^{+0.06}_{-0.07} M_\odot$ NS and a $\sim 8.21^{+0.77}_{-0.07} M_\odot$ BH with an aligned-spin of $\chi_{\text{BH}} \sim 0.62^{+0.06}_{-0.07}$. The merger would produce $\sim 0.005 - 0.03 M_\odot$ lanthanide-poor wind ejecta and $\sim 0.015 - 0.025 M_\odot$ lanthanide-rich dynamical ejecta. In Section 2.2, we suspected that GRB 211211A can be originated from NS-first-born NSBH mergers based on the estimations of the event rate density. Hu et al. (2022) found that for a NS-first-born NSBH binary system, the companion helium star would be tidally spun up efficiently by the NS, and would thus finally form a fast-spinning BH whose aligned-spin is always $\chi_{\text{BH}} \gtrsim 0.8$. Thus, the mass and spin of the BH component for GRB 211211A are essentially consistent with those of NS-first-born NSBH merger predicted by Hu et al. (2022).

Our fitting results show that the fall-back accretion for the interpretation of the EE starts at $t_0 = 11.2 \text{ s}$, peaks at $t_p = 30.2 \text{ s}$ and breaks around $t_b = 234 \text{ s}$ in the rest frame. The peak fall-back accretion rate is $\dot{M}_p \sim 2 \times 10^{-5} M_\odot \text{ s}^{-1}$. By Equation (4), one can estimate the fall-back mass as $M_{\text{fb}} \simeq \int_{t_0}^{t_b} \dot{M} dt \approx 1 \times 10^{-3} M_\odot$. The start time and peak accretion rate are consistent with the predictions by Desai et al. (2019). Furthermore, Desai et al. (2019) predicted that rebrightening EE caused by the fall-back accretion of r -process heating materials may only happen if the remnant BH has a mass of $\gtrsim 6 - 8 M_\odot$. Based on the fitting results, GRB 211211A would finally form a $\sim 10 M_\odot$ BH after the NSBH merger, so that our interpretations for the origin of GRB 211211A are self-consistent.

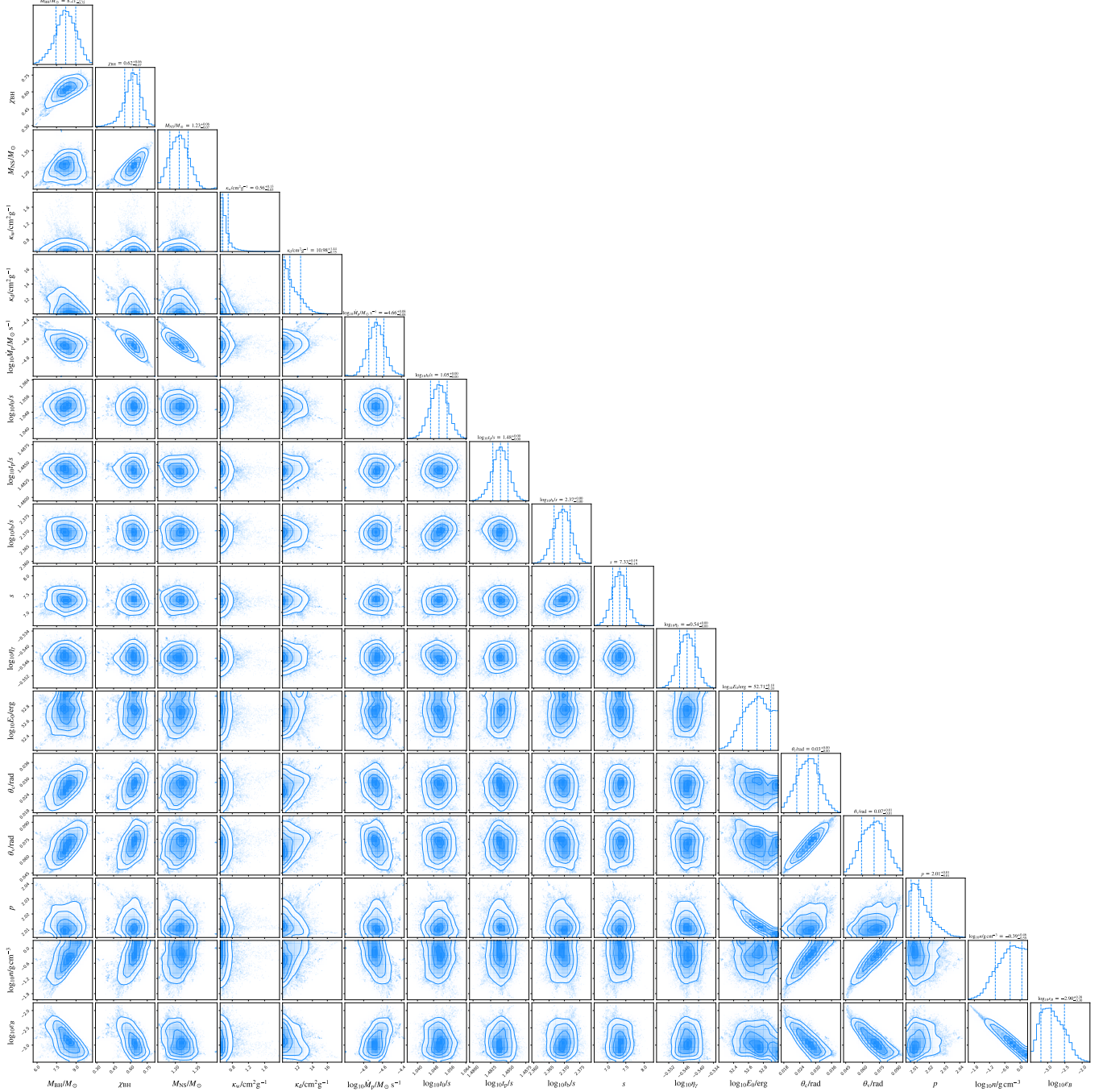


Figure 5. Posteriors of the fitting parameters. Medians and 1σ credible intervals are labeled.

There are some uncertainties in our fitting results. Our results reveal that the mass ratio between the BH and NS is ~ 7 for GRB 211211A. Due to present limited simulations for NS-first-born NSBH mergers, it is not sure if NSBH systems with such high mass ratio are common in the universe. More detailed simulations for the populations of NS-first-born NSBH mergers based on population synthesis and detailed binary evolution are suggested in the future. We also find $\sim 0.005 - 0.03 M_{\odot}$

lanthanide-poor wind ejecta is needed in order to explain the observations of the kilonova emission associated with GRB 211211A. A large amount of lanthanide-poor wind ejecta typically do not expect to be produced after NSBH mergers (e.g., Just et al. 2015; Fernández et al. 2015), although Fujibayashi et al. (2020) and Kyutoku et al. (2020) found that NSBH mergers still can lead to considerable lanthanide-poor wind ejecta if the viscous coefficient is not extremely high. Future multi-

messenger observations between NSBH GWs and associated kilonova emissions will help us constrain the mass fraction of r -process elements for the wind ejecta from NSBH mergers.

4. DISCUSSIONS AND CONCLUSION

In this *Letter*, we collect three unique merger-origin bursts, i.e., GRB 060614, GRB 211211, and GRB 211227A, to study their observed properties and explore possible origins. Both MEs and EEs of these bursts are long-duration, which fall into the distribution of IGRB populations. When the redshift information is considered, we find their WEs of these three bursts still behave as normal IGRBs, but their MEs lie on the sGRB track of the Amati relation. These similar observed properties are characterized differently than those of classical collapsar-origin IGRBs and merger-origin sGRBs with/without EEs, indicating a unique origin for these three bursts. Their X-ray MEs and EEs show unambiguous fall-back accretion signatures, decreasing as $\propto t^{-5/3}$, which extend the burst durations. The EEs might result from the fall-back of r -process heating materials, predicted to occur after NSBH mergers. The beaming-corrected local event rate density of these merger-origin IGRBs is estimated to be $\mathcal{R}_{0,b} \sim 2.4_{-1.3}^{+2.3}(f_b/0.01) \text{ Gpc}^{-3}\text{yr}^{-1}$. This local event rate density is much lower than that of BNS and NSBH mergers in the universe but consistent with the local event rate density of NS-first-born mergers.

Our detailed analysis on the EE using the fall-back accretion model, afterglow and kilonova of the recently high-impact event GRB 211211A reveals it could be a merger between a $\sim 1.23_{-0.07}^{+0.06} M_\odot$ NS and a $\sim 8.21_{-0.75}^{+0.77} M_\odot$ BH with a dimensionless aligned-spin parameter of $\chi_{\text{BH}} \sim 0.62_{-0.07}^{+0.06}$, supporting an NS-first-born NSBH formation channel. We find that the fall-back accretion for the interpretation of the EE starts at $t_0 = 11.2\text{s}$ and peaks at $t_p = 30.2\text{s}$ with a peak accretion rate of $\dot{M}_p \sim 2 \times 10^{-5} M_\odot \text{s}^{-1}$. The fall-back mass is $M_{\text{fb}} \sim 1 \times 10^{-3} M_\odot$. The start time and peak accretion rate are consistent with the fall-back accretion of r -process heating materials predicted by (Desai et al. 2019). After the completion of this *Letter*, we notice that Meng et al. (2022) also showed GRB 211211A can originate from a NSBH system in the photosphere emission model whose long duration is from the duration stretching effect of the saturated photosphere. Furthermore, Yang et al. (2015) reported that the kilonova candidate associated with GRB 060614 had an ejection of $\sim 0.1 M_\odot$ of r -process material. Yang et al. (2015) suggested that such significant ejected mass, within the possible range of dynamical ejecta of mergers between

NSs and BHs with extreme high aligned-spins (e.g., Lovelace et al. 2013; Kyutoku et al. 2015), strongly favored its origin for a NSBH merger rather than a BNS merger. Since NS-first-born NSBH mergers can easily occur tidal disruption while the rest of BH-first-born NSBH mergers mostly contribute to plunging events, NSBH mergers can well interpret the origins of these GRBs. Long-duration burst with rebrightening fall-back accretion signature of r -process heating materials after MEs, and bright kilonova emission might be commonly observed features for on-axis NSBH mergers.

Based on the estimated local event rate of merger-origin IGRBs, if they are certainly originated from NS-first-born NSBH mergers, the GW detection rate of NSBH mergers with fast-spinning primary BHs in the GW fourth observing run (O4) and fifth observing run (O5) of LIGO/Virgo/KAGRA Collaboration are $\sim 10 \text{ yr}^{-1}$ and $\sim 100 \text{ yr}^{-1}$ (Zhu et al. 2021b), respectively. By assuming that all of associated kilonova emissions can be detected, we estimate the multimessenger detection rate between GWs, GRB and kilonova emissions from NSBH mergers in O4 and O5 are $\sim 0.1(f_b/0.01) \text{ yr}^{-1}$ and $\sim 1(f_b/0.01) \text{ yr}^{-1}$, respectively. Thus, the smoking-gun evidence for NSBH merger origin of IGRB and kilonova will likely be verified in O5.

ACKNOWLEDGMENTS

The authors acknowledge an anonymous referee for useful discussions. We also thank Jun Yang, Bing Zhang, Bin-Bin Zhang, He Gao, Shun-Ke Ai, and Yun-Wei Yu for helpful comments. This work is supported by the National Natural Science Foundation of China (grant Nos. 11773003, 11833003, 12003028, 12103065, 12121003, 12133003, 12192220, 12192221, U1931201, U2038105), the National Basic Research Program of China (grant No. 2014CB845800), the China Manned Space Project (CMS-CSST-2021-B11), the Natural Science Foundation of Universities in Anhui Province (grant No. KJ2021A0106) and the National Key Research and Development Programs of China (2018YFA0404204).

Software: Python, <https://www.python.org/>; HEASoft (Nasa High Energy Astrophysics Science Archive Research Center (Heasarc) 2014), <http://heasarc.gsfc.nasa.gov/ftools/>; scikit-learn, <https://scikit-learn.org/stable/index.html>; emcee (Foreman-Mackey et al. 2013); corner (Foreman-Mackey 2016)

REFERENCES

- Abbott, B. P., Abbott, R., Abbott, T. D., et al. 2017a, *PhRvL*, 119, 161101
- . 2017b, *ApJL*, 848, L13
- . 2017c, *ApJL*, 848, L12
- . 2018, *PhRvL*, 121, 161101
- Abbott, R., Abbott, T. D., Abraham, S., et al. 2021a, *ApJL*, 915, L5
- . 2021b, *ApJL*, 913, L7
- Akmal, A., & Pandharipande, V. R. 1997, *PhRvC*, 56, 2261
- Amati, L., Frontera, F., Tavani, M., et al. 2002, *A&A*, 390, 81
- Anand, S., Coughlin, M. W., Kasliwal, M. M., et al. 2021, *Nature Astronomy*, 5, 46
- Andreoni, I., Kool, E. C., Sagués Carracedo, A., et al. 2020, *ApJ*, 904, 155
- Arcavi, I., Hosseinzadeh, G., Howell, D. A., et al. 2017, *Nature*, 551, 64
- Arnett, W. D. 1982, *ApJ*, 253, 785
- Bardeen, J. M., Press, W. H., & Teukolsky, S. A. 1972, *ApJ*, 178, 347
- Barnes, J., & Kasen, D. 2013, *ApJ*, 775, 18
- Belczynski, K., Klencki, J., Fields, C. E., et al. 2020, *A&A*, 636, A104
- Berger, E. 2007, *ApJ*, 670, 1254
- Blandford, R. D., & Znajek, R. L. 1977, *MNRAS*, 179, 433
- Bloom, J. S., Kulkarni, S. R., Harrison, F., et al. 1998, *ApJL*, 506, L105
- Bloom, J. S., Sigurdsson, S., & Pols, O. R. 1999, *MNRAS*, 305, 763
- Broekgaarden, F. S., & Berger, E. 2021, *ApJL*, 920, L13
- Broekgaarden, F. S., Berger, E., Neijssel, C. J., et al. 2021, *MNRAS*, 508, 5028
- Chang, X.-Z., Lü, H.-J., Chen, J.-M., & Liang, E.-W. 2022, *arXiv e-prints*, arXiv:2206.11438
- Chattopadhyay, D., Stevenson, S., Broekgaarden, F., Antonini, F., & Belczynski, K. 2022, *MNRAS*, 513, 5780
- Chattopadhyay, D., Stevenson, S., Hurley, J. R., Bailes, M., & Broekgaarden, F. 2021, *MNRAS*, 504, 3682
- Chatzopoulos, E., Wheeler, J. C., & Vinko, J. 2012, *ApJ*, 746, 121
- Chevalier, R. A. 1998, *ApJ*, 499, 810
- Christensen, L., Hjorth, J., & Gorosabel, J. 2004, *A&A*, 425, 913
- Coughlin, M. W., Dietrich, T., Antier, S., et al. 2020, *MNRAS*, 497, 1181
- Coulter, D. A., Foley, R. J., Kilpatrick, C. D., et al. 2017, *Science*, 358, 1556
- Dai, Z. G., & Liu, R.-Y. 2012, *ApJ*, 759, 58
- Darbha, S., Kasen, D., Foucart, F., & Price, D. J. 2021, *ApJ*, 915, 69
- D’Avanzo, P., Malesani, D., Covino, S., et al. 2009, *A&A*, 498, 711
- Della Valle, M., Chincarini, G., Panagia, N., et al. 2006, *Nature*, 444, 1050
- Deng, C.-M. 2020, *MNRAS*, 497, 643
- Desai, D., Metzger, B. D., & Foucart, F. 2019, *MNRAS*, 485, 4404
- Di Clemente, F., Drago, A., & Pagliara, G. 2022, *ApJ*, 929, 44
- D’Orazio, D. J., Haiman, Z., Levin, J., Samsing, J., & Vigna-Gómez, A. 2022, *ApJ*, 927, 56
- Drout, M. R., Piro, A. L., Shappee, B. J., et al. 2017, *Science*, 358, 1570
- Drozda, P., Belczynski, K., O’Shaughnessy, R., Bulik, T., & Fryer, C. L. 2020, *arXiv e-prints*, arXiv:2009.06655
- Eichler, D., Livio, M., Piran, T., & Schramm, D. N. 1989, *Nature*, 340, 126
- Evans, P. A., Cenko, S. B., Kennea, J. A., et al. 2017, *Science*, 358, 1565
- Fernández, R., Foucart, F., Kasen, D., et al. 2017, *Classical and Quantum Gravity*, 34, 154001
- Fernández, R., Kasen, D., Metzger, B. D., & Quataert, E. 2015, *MNRAS*, 446, 750
- Fong, W., Berger, E., & Fox, D. B. 2010, *ApJ*, 708, 9
- Fong, W., Berger, E., Margutti, R., & Zauderer, B. A. 2015, *ApJ*, 815, 102
- Foreman-Mackey, D. 2016, *The Journal of Open Source Software*, 1, 24. <https://doi.org/10.21105/joss.00024>
- Foreman-Mackey, D., Hogg, D. W., Lang, D., & Goodman, J. 2013, *PASP*, 125, 306
- Foucart, F., Hinderer, T., & Nissanke, S. 2018, *PhRvD*, 98, 081501
- Fragione, G. 2021, *ApJL*, 923, L2
- Fujibayashi, S., Shibata, M., Wanajo, S., et al. 2020, *PhRvD*, 101, 083029
- Gal-Yam, A., Fox, D. B., Price, P. A., et al. 2006, *Nature*, 444, 1053
- Galama, T. J., Vreeswijk, P. M., van Paradijs, J., et al. 1998, *Nature*, 395, 670
- Gao, H., Lei, W.-H., & Zhu, Z.-P. 2022, *arXiv e-prints*, arXiv:2205.05031
- Gehrels, N. 1986, *ApJ*, 303, 336
- Ghirlanda, G., Salafia, O. S., Paragi, Z., et al. 2019, *Science*, 363, 968
- Giacobbo, N., & Mapelli, M. 2018, *MNRAS*, 480, 2011
- Goldstein, A., Veres, P., Burns, E., et al. 2017, *ApJL*, 848, L14

- Goldstein, A., Hamburg, R., Wood, J., et al. 2019, arXiv e-prints, arXiv:1903.12597
- Gompertz, B. P., Levan, A. J., & Tanvir, N. R. 2020a, *ApJ*, 895, 58
- Gompertz, B. P., Nicholl, M., Schmidt, P., Pratten, G., & Vecchio, A. 2022a, *MNRAS*, 511, 1454
- Gompertz, B. P., Cutter, R., Steeghs, D., et al. 2020b, *MNRAS*, 497, 726
- Gompertz, B. P., Ravasio, M. E., Nicholl, M., et al. 2022b, arXiv e-prints, arXiv:2205.05008
- Gruber, D., Goldstein, A., Weller von Ahlefeld, V., et al. 2014, *ApJS*, 211, 12
- Hu, R.-C., Zhu, J.-P., Qin, Y., et al. 2022, *ApJ*, 928, 163
- Just, O., Bauswein, A., Ardevol Pulpillo, R., Goriely, S., & Janka, H. T. 2015, *MNRAS*, 448, 541
- Kasen, D., Metzger, B., Barnes, J., Quataert, E., & Ramirez-Ruiz, E. 2017, *Nature*, 551, 80
- Kasliwal, M. M., Nakar, E., Singer, L. P., et al. 2017, *Science*, 358, 1559
- Kasliwal, M. M., Anand, S., Ahumada, T., et al. 2020, *ApJ*, 905, 145
- Kawaguchi, K., Kyutoku, K., Shibata, M., & Tanaka, M. 2016, *ApJ*, 825, 52
- Kawaguchi, K., Shibata, M., & Tanaka, M. 2020, *ApJ*, 889, 171
- Kilpatrick, C. D., Foley, R. J., Kasen, D., et al. 2017, *Science*, 358, 1583
- Korobkin, O., Rosswog, S., Arcones, A., & Winteler, C. 2012, *MNRAS*, 426, 1940
- Kouveliotou, C., Meegan, C. A., Fishman, G. J., et al. 1993, *ApJL*, 413, L101
- Kumar, P., & Zhang, B. 2015, *PhR*, 561, 1
- Kyutoku, K., Fujibayashi, S., Hayashi, K., et al. 2020, *ApJL*, 890, L4
- Kyutoku, K., Ioka, K., Okawa, H., Shibata, M., & Taniguchi, K. 2015, *PhRvD*, 92, 044028
- Lamb, G. P., & Kobayashi, S. 2018, *MNRAS*, 478, 733
- Lamb, G. P., Lyman, J. D., Levan, A. J., et al. 2019, *ApJL*, 870, L15
- Lan, L., Lu, R.-J., Lü, H.-J., et al. 2020, *MNRAS*, 492, 3622
- Lattimer, J. M. 2012, *Annual Review of Nuclear and Particle Science*, 62, 485
- Lattimer, J. M., & Schramm, D. N. 1974, *ApJL*, 192, L145
- . 1976, *ApJ*, 210, 549
- Lazzati, D., Perna, R., Morsony, B. J., et al. 2018, *PhRvL*, 120, 241103
- Lei, W.-H., Zhang, B., & Liang, E.-W. 2013, *ApJ*, 765, 125
- Lei, W.-H., Zhang, B., Wu, X.-F., & Liang, E.-W. 2017, *ApJ*, 849, 47
- Li, L.-X., & Paczyński, B. 1998, *ApJL*, 507, L59
- . 2000, *ApJL*, 534, L197
- Li, Y., Zhang, B., & Lü, H.-J. 2016, *ApJS*, 227, 7
- Liu, T., Gu, W.-M., & Zhang, B. 2017, *NewAR*, 79, 1
- Liu, T., Liang, E.-W., Gu, W.-M., et al. 2012, *ApJ*, 760, 63
- Lovelace, G., Duez, M. D., Foucart, F., et al. 2013, *Classical and Quantum Gravity*, 30, 135004
- Lü, H.-J., Yuan, H.-Y., Yi, T.-F., et al. 2022, *ApJL*, 931, L23
- Lyman, J. D., Lamb, G. P., Levan, A. J., et al. 2018, *Nature Astronomy*, 2, 751
- MacFadyen, A. I., Woosley, S. E., & Heger, A. 2001, *ApJ*, 550, 410
- Mandel, I., & Broekgaarden, F. S. 2022, *Living Reviews in Relativity*, 25, 1
- Mandel, I., & Smith, R. J. E. 2021, *ApJL*, 922, L14
- Margutti, R., Berger, E., Fong, W., et al. 2017, *ApJL*, 848, L20
- Mei, A., Banerjee, B., Oganessian, G., et al. 2022, arXiv e-prints, arXiv:2205.08566
- Meng, Y. Z., Wang, X. I., & Liu, Z. K. 2022, in preparation.
- Metzger, B. D., Arcones, A., Quataert, E., & Martínez-Pinedo, G. 2010a, *MNRAS*, 402, 2771
- Metzger, B. D., Martínez-Pinedo, G., Darbha, S., et al. 2010b, *MNRAS*, 406, 2650
- Minaev, P. Y., & Pozanenko, A. S. 2020, *MNRAS*, 492, 1919
- Mooley, K. P., Deller, A. T., Gottlieb, O., et al. 2018, *Nature*, 561, 355
- Narayan, R., Paczynski, B., & Piran, T. 1992, *ApJL*, 395, L83
- Narayana Bhat, P., Meegan, C. A., von Kienlin, A., et al. 2016, *ApJS*, 223, 28
- Nasa High Energy Astrophysics Science Archive Research Center (Heasarc). 2014, HEASoft: Unified Release of FTOOLS and XANADU, Astrophysics Source Code Library, record ascl:1408.004, , ascl:1408.004
- Nitz, A. H., Kumar, S., Wang, Y.-F., et al. 2021, arXiv e-prints, arXiv:2112.06878
- Norris, J. P., & Bonnell, J. T. 2006, *ApJ*, 643, 266
- Norris, J. P., Cline, T. L., Desai, U. D., & Teegarden, B. J. 1984, *Nature*, 308, 434
- Novikov, I. D., & Thorne, K. S. 1973, in *Black Holes (Les Astres Occlus)*, 343–450
- Paczynski, B. 1986, *ApJL*, 308, L43
- . 1991, *AcA*, 41, 257
- Page, K. L., Evans, P. A., Tohuvavohu, A., et al. 2020, *MNRAS*, 499, 3459
- Perego, A., Radice, D., & Bernuzzi, S. 2017, *ApJL*, 850, L37
- Pian, E., D’Avanzo, P., Benetti, S., et al. 2017, *Nature*, 551, 67

- Planck Collaboration, Aghanim, N., Akrami, Y., et al. 2020, *A&A*, 641, A6
- Proga, D., & Zhang, B. 2006, *MNRAS*, 370, L61
- Rastinejad, J. C., Gompertz, B. P., Levan, A. J., et al. 2022, arXiv e-prints, arXiv:2204.10864
- Rees, M. J. 1988, *Nature*, 333, 523
- Román-Garza, J., Bavera, S. S., Fragos, T., et al. 2021, *ApJL*, 912, L23
- Rosswog, S. 2007, *MNRAS*, 376, L48
- Ruiz, M., Paschalidis, V., Tsokaros, A., & Shapiro, S. L. 2020, *PhRvD*, 102, 124077
- Sagués Carracedo, A., Bulla, M., Feindt, U., & Goobar, A. 2021, *MNRAS*, 504, 1294
- Sari, R., Piran, T., & Narayan, R. 1998, *ApJL*, 497, L17
- Savchenko, V., Ferrigno, C., Kuulkers, E., et al. 2017, *ApJL*, 848, L15
- Shao, Y., & Li, X.-D. 2021, *ApJ*, 920, 81
- Shapiro, S. L. 2017, *PhRvD*, 95, 101303
- Siegel, D. M., & Metzger, B. D. 2017, *PhRvL*, 119, 231102
- Smartt, S. J., Chen, T. W., Jerkstrand, A., et al. 2017, *Nature*, 551, 75
- Sun, H., Zhang, B., & Li, Z. 2015, *ApJ*, 812, 33
- Sun, H., Liu, H.-Y., Pan, H.-W., et al. 2022, *ApJ*, 927, 224
- Symbalisty, E., & Schramm, D. N. 1982, *Astrophys. Lett.*, 22, 143
- The LIGO Scientific Collaboration, the Virgo Collaboration, the KAGRA Collaboration, et al. 2021, arXiv e-prints, arXiv:2111.03634
- Troja, E., Piro, L., van Eerten, H., et al. 2017, *Nature*, 551, 71
- Troja, E., Piro, L., Ryan, G., et al. 2018, *MNRAS*, 478, L18
- Tsvetkova, A., Frederiks, D., Lysenko, A., et al. 2022, *GRB Coordinates Network*, 31544, 1
- Tunnicliffe, R. L., & Levan, A. 2012, in *Death of Massive Stars: Supernovae and Gamma-Ray Bursts*, ed. P. Roming, N. Kawai, & E. Pian, Vol. 279, 415–416
- von Kienlin, A., Meegan, C. A., Paciesas, W. S., et al. 2014, *ApJS*, 211, 13
- . 2020, *ApJ*, 893, 46
- Waxman, E., Ofek, E. O., & Kushnir, D. 2022, arXiv e-prints, arXiv:2206.10710
- Woosley, S. E., & Bloom, J. S. 2006, *ARA&A*, 44, 507
- Wu, X.-F., Hou, S.-J., & Lei, W.-H. 2013, *ApJL*, 767, L36
- Xiao, S., Zhang, Y.-Q., Zhu, Z.-P., et al. 2022, arXiv e-prints, arXiv:2205.02186
- Xie, X., Zrake, J., & MacFadyen, A. 2018, *ApJ*, 863, 58
- Yang, B., Jin, Z.-P., Li, X., et al. 2015, *Nature Communications*, 6, 7323
- Yang, J., Zhang, B. B., Ai, S. K., et al. 2022, arXiv e-prints, arXiv:2204.12771
- Yang, Y.-S., Zhong, S.-Q., Zhang, B.-B., et al. 2020, *ApJ*, 899, 60
- Zaninoni, E., Bernardini, M. G., Margutti, R., & Amati, L. 2016, *MNRAS*, 455, 1375
- Zhang, B. 2018, *The Physics of Gamma-Ray Bursts*, doi:10.1017/9781139226530
- . 2019, *Frontiers of Physics*, 14, 64402
- Zhang, B., & Mészáros, P. 2001, *ApJL*, 552, L35
- . 2002, *ApJ*, 571, 876
- Zhang, B., Zhang, B.-B., Liang, E.-W., et al. 2007, *ApJL*, 655, L25
- Zhang, B., Zhang, B.-B., Virgili, F. J., et al. 2009, *ApJ*, 703, 1696
- Zhang, B. B., Zhang, B., Sun, H., et al. 2018, *Nature Communications*, 9, 447
- Zhang, H.-M., Huang, Y.-Y., Zheng, J.-H., Liu, R.-Y., & Wang, X.-Y. 2022, arXiv e-prints, arXiv:2205.09675
- Zhu, J.-P., Wu, S., Qin, Y., et al. 2022, *ApJ*, 928, 167
- Zhu, J.-P., Wu, S., Yang, Y.-P., et al. 2021a, *ApJ*, 921, 156
- Zhu, J.-P., Yang, Y.-P., Liu, L.-D., et al. 2020, *ApJ*, 897, 20
- Zhu, J.-P., Wu, S., Yang, Y.-P., et al. 2021b, *ApJ*, 917, 24